A Quantum-dot-based CMOS Image Sensor with Direct X-ray Conversion for Nondestructive Testing

Chun-Min Zhang, Riccardo Quaglia, Artem Shulga, Vincent Goossens, Paula Blanca Cruz, Rémy Vuagniaux, and Pierre-François Rüedi

***Abstract*—This paper presents the promising use of our newly developed X-ray image sensor in nondestructive test for industrial inspection. It consists of an absorber stack with a 120-μm layer of lead sulfide (PbS) colloidal quantum dots (CQDs) monolithically and directly deposited on a CMOS readout chip. This combination leverages both CMOS processes and PbS CQDs to achieve high X-ray absorption efficiency, thin-film integration, low power consumption, high pixel resolution, efficient readout electronics, and a 100% fill factor. To the best of our knowledge, this is the first direct X-ray CMOS image sensor that utilizes PbS CQDs to convert X-rays directly into electrical signals, which are then processed by CMOS readout circuitry for efficient signal handling.**

***Index Terms*—CMOS readout, colloidal quantum dots, composite materials, CQDs, direct conversion, industrial inspection, lead sulfide, monolithic integration, nondestructive test, NDT, PCB, printed circuit boards, PbS, quantum dots, X-ray imaging**

I. Introduction

Since Röntgen's discovery of X-ray's ability to penetrate matter in 1895, X-ray sensing technologies have evolved from early X-ray tubes and radiographic films to modern computed tomography and digital radiography, with widespread applications in medical diagnostics, industrial inspection, and security screening [1]. Most contemporary X-ray image sensors rely on scintillators–such as cesium iodide (CsI) or gadolinium oxysulfide (Gd_2O_2S)–to convert incident X-rays into visible or near-visible photons, which are then detected by photodiode arrays and translated into electrical signals. However, this indirect-conversion approach is limited by signal loss during photon conversion and reduced spatial resolution due to optical crosstalk between adjacent pixels [2]. In contrast, direct-conversion detectors based on cadmium telluride (CdTe), cadmium zinc telluride (CdZnTe), or amorphous-selenium (α-Se) eliminate the need for the scintillator by converting X-rays directly into electrical charges, thereby improving both absorption efficiency and spatial resolution [2]. Nonetheless, in addition to costly material manufacturing processes, Cd[Zn]Te devices require flip-chip hybridization to interface with CMOS electronics, introducing assembly complexity and limiting achievable pixel resolution [3]. Meanwhile, α-Se, due to its low atomic number, exhibits limited stopping power for high-energy X-rays, restricting its effective use to low-energy imaging applications, such as mammography at 20-30 keV [4].

Lead sulfide (PbS) colloidal quantum dots (CQDs) are chemically synthesized semiconductor nanocrystals that can be solution-processed at low temperatures without requiring high-vacuum conditions. Owing to its high X-ray absorption efficiency with the high atomic number, a PbS-CQD layer as thin as 120 μm is sufficient to absorb a broad range of X-rays [5]. Furthermore, PbS CQDs enable the fabrication of efficient absorber stacks directly on CMOS readout chips, supporting low power consumption, high pixel resolution, complex readout electronics, and a 100% fill factor [6]. We have developed a direct-conversion X-ray image sensor using a monolithically integrated PbS-CQD absorber stack deposited directly onto a CMOS readout chip. This technology was initially targeted for nondestructive test (NDT) of invisible defects and structural health monitoring in composite materials, which are increasingly adopted in aerospace applications for their lightweight and robust mechanical properties. Building upon our initial demonstration in a recent letter [7], we now present a comprehensive study of this first monolithic thin-film X-ray sensing technology and explore its potential for industrial inspection in NDT applications.

II. Sensor architecture

Fig. 1a illustrates the design concept and fabrication process of the proposed direct-conversion X-ray image sensor, featuring solution-based monolithic integration of a PbS-CQD-based photon absorber on a CMOS readout chip. The fabrication flow includes readout chip tapeout, PbS CQD synthesis, ink formation, and solution-based layer deposition. The absorber stack utilizes the top metal layer of CMOS processes as the in-pixel electrode, followed by a 100-nm zinc-oxide (ZnO) nanoparticle layer for electron transport, a 120-μm PbS-CQD layer for broadband X-ray absorption, a less than 100-nm layer of poly[bis(4-phenyl)(2,4,6-trimethylphenyl)amine] (PTAA) for hole transport, and a 60-nm gold layer serving as the global top electrode. Except for the contacting layers, all materials are solution-processed, with PbS CQDs deposited via spray coating. As shown in Fig. 1b, a PbS layer demonstrates higher X-ray absorption

This work has received funding from the Clean Sky 2 Joint Undertaking program under grant agreement No. 887192 and the Swiss State Secretariat for Education, Research, and Innovation (SERI) under the SwissChips initiative. Chun-Min Zhang, Riccardo Quaglia, Paula Blanca Cruz, Rémy Vuagniaux, and Pierre-François Rüedi are with the Edge AI & Vision Systems Group, Centre Suisse d'Electronique et de Microtechnique (CSEM), Neuchâtel, 2002, Switzerland. Vincent Goossens and Artem Shulga are with QDI Systems, Groningen, 9713, The Netherlands.

Corresponding author: Chun-Min Zhang (email: chun-min.zhang@csem.ch; Tel.: +41 32 720 59 81).

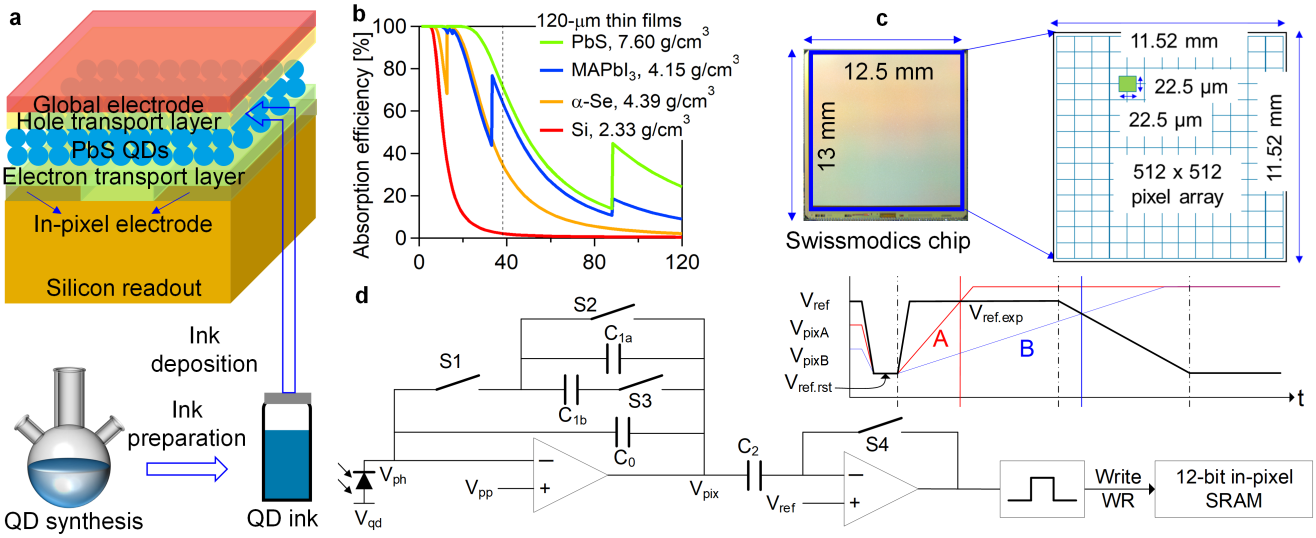

Fig. 1: Sensor design and fabrication: (a) sensor architecture featuring solution-processed monolithic integration of a PbS-CQD-based absorber stack on a CMOS readout chip; (b) X-ray absorption efficiency comparison across sensing materials, with a bulk PbS crystal layer demonstrating superior performance; (c) CMOS readout comprising a 512 x 512 pixel array and a 22.5-µm pixel pitch; (d) pixel-level circuitry including a charge-sensitive preamplifier, configurable integration capacitors, a capacitively coupled comparator, and a time-to-digital converter with 12-bit in-pixel memory. Note that V_{qd} and V_{ph} are the biases at the global top electrode and the in-pixel electrode, respectively.

efficiency across a broad energy range compared to silicon, α-Se, and organic-inorganic lead halide perovskites ($MAPbI_3$) of the same thickness. For composite material inspection, low-energy X-rays in the range of 10-40 keV, where the 120-µm PbS layer achieves near-complete absorption, provides optimal contrast. Note that the calculation here corresponds to a bulk PbS crystal layer which has a higher density than a less-packed PbS-CQD layer.

The CMOS readout chip was designed and fabricated using a 180-nm CMOS process and features a chip area of 13 mm x 12.5 mm, a 512 x 512 pixel array, and a 22.5-µm pixel pitch (Fig. 1c). The pixel architecture (Fig. 1d) integrates a charge-sensitive preamplifier, configurable integration capacitors, a capacitively coupled comparator, and a time-to-digital converter with 12-bit in-pixel memory. Multiple conversion gains (CGs) are supported via capacitor configuration, allowing adaptation to various photon energies. To achieve a wide dynamic range within limited bit depth, the readout employs a time-to-digital conversion scheme combining logarithmic encoding over a constant reference voltage (V_{ref}) and a linear ramp phase to perform analog-to-digital conversion for remaining pixels. Further details are available in [7].

III. Function Verification

We employed the developed image sensor to scan sensor boards and a portion of a smartphone, demonstrating its X-ray imaging functionality for printed circuit board (PCB) inspection. As shown in Fig. 2a, the setup consists of an imaging system integrated with a compact XY scanning stage, allowing scanning of boards larger than the sensor's active area. The dark region in Fig. 2b–compared with the

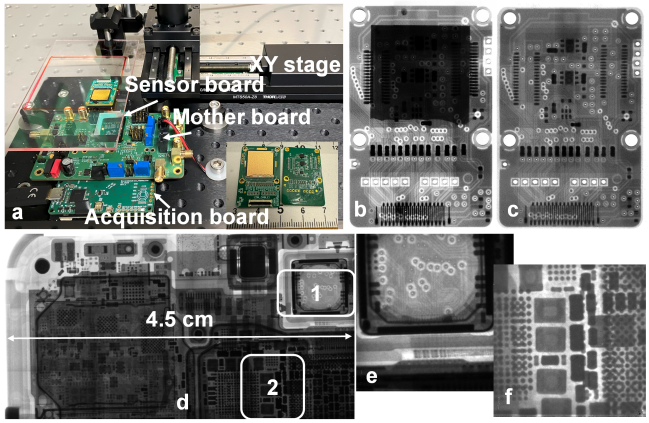

Fig. 2: Nondestructive test of PCBs: (a) experimental setup with a compact XY scanning stage used to image sensor boards–one with a coated chip (left in the insert) and one without any chip (right in the insert); (b, c) stitched X-ray images of two sensor boards acquired at a tube voltage (V_{tube}) of 60 kV and top biases (V_{qd}) of −16 V and −6.5 V, respectively; (d) a stitched X-ray image of a partial smartphone scan under 80 kV of V_{tube} and −16 V of V_{qd}; (e, f) high-contrast X-ray images corresponding to regions 1 and 2 in (d).

corresponding area of a chip-free board in Fig. 2c–indicates the presence of the QD-coated chip, confirming efficient X-ray absorption by our senor. Furthermore, Fig. 2d and Fig. 2e-h also reveal the sensor's ability to visualize not only surface-mounted electronic components but also internal structures, including interlayer connections and wiring, underscoring its

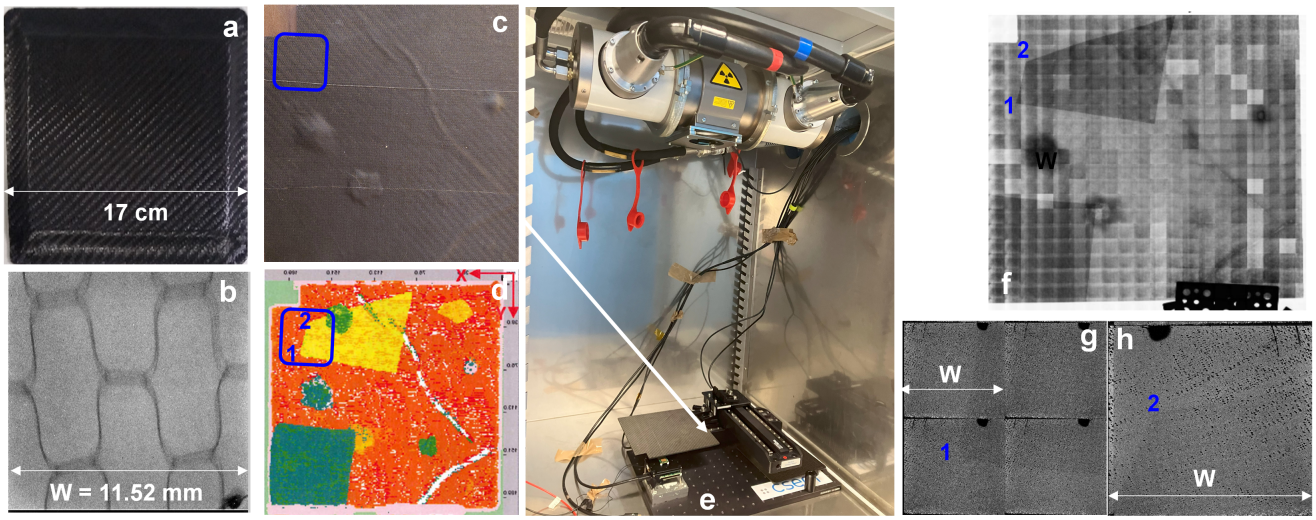

Fig. 3: Nondestructive test of composite materials: (a) a smartphone photo of a 1.5-cm-thick carbon composite sample; (b) its corresponding X-ray image acquired at 40 kV of V_{tube} and −10 V of V_{qd}; (c) a smartphone photo of a carbon prepreg sample with embedded defects; (d) its reference ultrasound cartography; (e) X-ray imaging setup for scanning the entire sample; (f) an stitched X-ray image of the full sample obtained at 28 kV of V_{tube} and −12 V of V_{qd}; (g, h) X-ray images of a Teflon-included region, scanned at 20 kV of V_{tube} and −5 V of V_{qd}. Black spots correspond to the global top electrode.

potential for high-resolution PCB inspection.

Aircraft undergo regular inspections during routine maintenance or following impacts from ground support equipment or bird strikes during flight [8]. Detecting defects in composite structures–now a major component of modern aircraft (e.g., the Boeing 787 [9]) owing to their light weight with robust mechanical properties ([10])–is critically important. Various DNT methods are employed to identify hidden defects such as voids and delamination, supporting risk assessment and airworthiness evaluation [8]. However, conventional techniques often require grounding and partial disassembly–processes that are time-consuming and costly [11]. Our thin-film X-ray image sensor was originally proposed as an integrated solution for contact-based health monitoring of composite structures at high-risk locations. This approach has the potential to significantly reduce inspection time and minimize last-minute operational disruptions.

Fig. 3 summarizes the results of NDT of composite materials. The honeycomb structure of a defect-free composite sample (Fig. 3a) is clearly visible in its corresponding X-ray image (Fig. 3b). To further demonstrate diagnostic capability, we tested a carbon prepreg sample with intentionally introduced defects–including inclusions, wrinkling, and delamination. A smartphone photo (Fig. 3c) and an ultrasound cartography image (Fig. 3d) serve as ground-truth references. Given the large surface area of the sample relative to the senor's active area, we implemented an automated scanning setup with a large XY stage, integrated with image acquisition via a MATLAB script (Fig. 3e). The captured sub-images were stitched and processed using a Python script to generate a complete view of the sample. Image processing steps included flat-field correction using averaged frames, artifact and grid pattern removal through frequency filtering, and manual contrast adjustments.

The resulting stitched X-ray image (Fig. 3f) reveals nearly all embedded defects–including folding, a foam block, dry carbon fiber, Teflon, and protective prepreg paper–with the exception of bubble wrap. To provide higher clarity without interference from grid artifacts, we also present high-resolution scans of the Teflon region corners (Fig. 3g, h). Sensor fabrication has progressed toward improved uniformity, with certain sensors yielding better, though still partial, imaging results. These outcomes indicate strong potential for further optimization and enhanced performance in future iterations. Given that defects such as porosity, voids, and inclusions are known to occur during composite manufacturing [10], the demonstrated thin-film X-ray imaging approach may offer potential for integration into production

TABLE I: Sensor features and applied setting

Chip architecture	PbS CQDs/CMOS ROICs
QD film thickness	120 µm
Pixel pitch	22.5 µm
Pixel resolution	512 x 512
Sensitive area	11.52 mm x 11.52 mm
Fill factor	100%
Shutter type	Global shutter
Frame rate	50 fps
Signal conversion	Direct X-ray conversion
Polarity	Electron collection
Conversion gain (CG)	53 µV/e^- (high CG)
Full-well capacity	18.7 ke^- (high CG)
Dark-signal non-uniformity	26 e^- (high CG)
Temporal noise	50 e^- (high CG)
Dark current	2.79 nA/cm^2 at a top bias of −6 V
Power consumption	63 mW
Readout interface	Parallel and serial data transmission

Note: The CMOS readout chip can also be used for hole collection and includes low CGs when adding C_{1a} and C_{1b}.

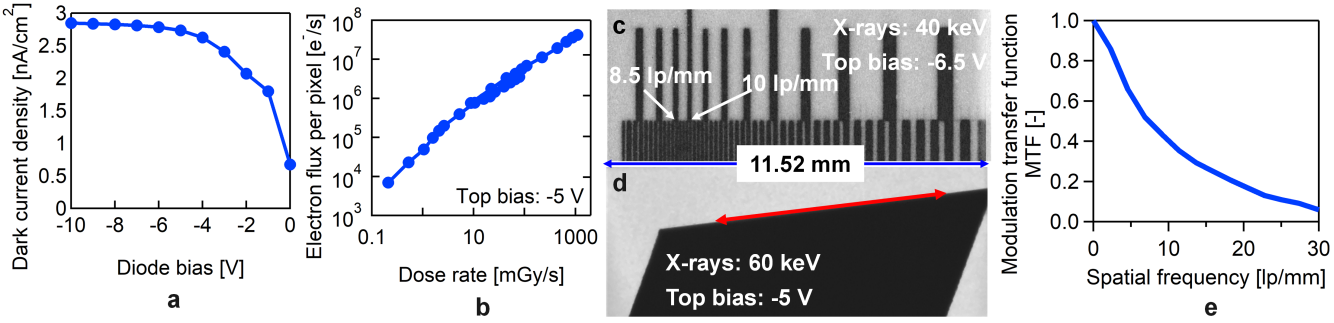

Fig. 4: Sensor characterization: (a) dark current density with respect to the bias across the absorber stack; (b) linear response with respect to a wide range of dose rate; (c) an X-ray image of a line pattern; (d) an X-ray image of an edge of a slanted edge for extracting MTF; (e) extracted MTF with respect to spatial frequency.

environments to support real-time quality monitoring.

IV. Sensor Characterization

While demonstrating imaging functionality across various scenarios, we have also been performing systematic sensor characterization. Table I summarizes key sensor features and experimental settings. This image sensor offers a 100% fill factor, a global shutter, low dark current, multiple CGs, electron and hole collection, and both parallel and serial data buses. This study uses electron collection and the highest CG. Fig. 4 presents fundamental characterization results. As shown in Fig. 4a, the dark current density increases with the bias at the global top electrode and saturates below 3 nA/cm^2. The sensor exhibits a linear response to dose rate over four orders of magnitude (Fig. 4b). A high-contrast X-ray image of a line pattern (Fig. 4c) demonstrates spatial resolution of at least 10 line pairs per millimeter (lp/mm). The modulation transfer function (MTF) was calculated using the slanted edge method. A straight edge image (Fig. 4d) was normalized and projected along the direction perpendicular to the edge to obtain the edge spread function (ESF). The ESF was binned into intervals of 0.3 pixels, and its derivative was computed to derive the line spread function (LSF). The Fourier transform of the LSF yielded the MTF. As shown in Fig. 4e, the MTF10 (10% modulation level) reaches up to 22 lp/mm, closely matching the theoretical resolution limit.

V. Conclusion

We have developed what is, to our knowledge, the first monolithic thin-film direct X-ray image sensor that integrates a CMOS readout chip with a solution-processed PbS-CQD-based absorber stack. This sensor exhibits promising X-ray detection performance, characterized by low dark current, high X-ray sensitivity, and high spatial resolution. Experimental validation demonstrates its potential for nondestructive testing of printed circuit boards and composite materials in industrial inspection applications. This initial demonstration of solution-based monolithic integration highlights a viable path toward cost-effective, high-performance X-ray detectors.

Acknowledgements

We thank Hans-Rudolf Graf and Loïc Zahnd for their contribution to digital IC design, Dr. Patrick Stadelmann for the support with firmware, and Eric Grenet and Yves Cainaud for arranging the XY stage. We thank Almay Technologies for providing us with composite samples for function verification. And we thank Université Jean Monnet and ISAE-SUPAERO for letting us access their X-ray instruments, especially Alexandre Neyret for his support in image acquisition.

References

[1] X. Ou, X. Chen, X. Xu, L. Xie, X. Chen, Z. Hong, H. Bai, X. Liu, Q. Chen, L. Li, and H. Yang, "Recent development in X-ray imaging technology: Future and challenges," *Research*, vol. 2021, 2021.

[2] M. Overdick, C. Baumer, K. J. Engel, J. Fink, C. Herrmann, H. Kruger, M. Simon, R. Steadman, and G. Zeitler, "Status of direct conversion detectors for medical imaging with X-rays," *IEEE Transactions on Nuclear Science*, vol. 56, no. 4, pp. 1800–1809, 2009.

[3] Y. Oike, "Evolution of image sensor architectures with stacked device technologies," *IEEE Transactions on Electron Devices*, vol. 69, no. 6, pp. 2757–2765, 2022.

[4] A. Datta, Z. Zhong, and S. Motakef, "A new generation of direct X-ray detectors for medical and synchrotron imaging applications," *Scientific Reports*, vol. 10, no. 1, p. 20097, 2020.

[5] M. Yarema, O. Yarema, W. M. M. Lin, S. Volk, N. Yazdani, D. Bozyigit, and V. Wood, "Upscaling colloidal nanocrystal hot-injection syntheses via reactor underpressure," *Chemistry of Materials*, vol. 29, no. 2, pp. 796–803, 2017.

[6] M. T. Bohr and I. A. Young, "CMOS scaling trends and beyond," *IEEE Micro*, vol. 37, no. 6, pp. 20–29, 2017.

[7] C.-M. Zhang, R. Quaglia, A. Shulga, V. Goossens, P. B. Cruz, and P.-F. Rüedi, "A quantum-dot-coated CMOS image sensor with a wide-spectral sensitivity from X-rays to SWIR photons," *IEEE Sensors Letters*, vol. 8, no. 8, pp. 1–4, 2024.

[8] H. Towsyfyan, A. Biguri, R. Boardman, and T. Blumensath, "Successes and challenges in non-destructive testing of aircraft composite structures," *Chinese Journal of Aeronautics*, vol. 33, no. 3, pp. 771–791, 2020.

[9] J. of Young Investigators, "The Boeing 787 Dreamliner: Designing an aircraft for the future," https://www.jyi.org/2010-august/2010/8/6/the-boeing-787-dreamliner-designing-an-aircraft-for-the-future, [Online; accessed Apr. 3, 2024].

[10] B. Parveez, M. Kittur, I. A. Badruddin, S. Kamangar, M. Hussien, and M. Umarfarooq, "Scientific advancements in composite materials for aircraft applications: a review," *Polymers*, vol. 14, no. 22, p. 5007, 2022.

[11] I. C. Metz, J. Ellerbroek, T. Mühlhausen, D. Kügler, and J. M. Hoekstra, "The bird strike challenge," *Aerospace*, vol. 7, no. 3, p. 26, 2020.